Probing Operator Spreading via Floquet Engineering in a Superconducting Circuit

S. K. Zhao, Zi-Yong Ge, Zhongcheng Xiang, G. M. Xue, H. S. Yan, Z. T. Wang, Zhan Wang,
H. K. Xu, F. F. Su, Z. H. Yang, He Zhang, Yu-Ran Zhang, Xue-Yi Guo, Kai Xu, Ye Tian, H. F. Yu,
D. N. Zheng, Heng Fan, and S. P. Zhao

Probing Operator Spreading via Floquet Engineering in a Superconducting Circuit

S. K. Zhao,[1,2,3,*] Zi-Yong Ge,[1,2,*] Zhongcheng Xiang,[1,*] G. M. Xue,[3] H. S. Yan,[1,2] Z. T. Wang,[1,2]
Zhan Wang,[1,2] H. K. Xu,[3] F. F. Su,[1] Z. H. Yang,[1,2] He Zhang,[1,2] Yu-Ran Zhang,[4] Xue-Yi Guo,[1]
Kai Xu,[1,3,5] Ye Tian,[1] H. F. Yu,[3,†] D. N. Zheng,[1,2,5,6,‡] Heng Fan,[1,2,3,5,6,§] and S. P. Zhao[1,2,5,6,¶]

[1]*Beijing National Laboratory for Condensed Matter Physics,
Institute of Physics, Chinese Academy of Sciences, Beijing 100190, China*
[2]*School of Physical Sciences, University of Chinese Academy of Sciences, Beijing 100190, China*
[3]*Beijing Academy of Quantum Information Sciences, Beijing 100193, China*
[4]*Theoretical Quantum Physics Laboratory, RIKEN Cluster for Pioneering Research, Wako-shi, Saitama 351-0198, Japan*
[5]*CAS Center for Excellence in Topological Quantum Computation, UCAS, Beijing 100190, China*
[6]*Songshan Lake Materials Laboratory, Dongguan 523808, China*

Operator spreading, often characterized by out-of-time-order correlators (OTOCs), is one of the central concepts in quantum many-body physics. However, measuring OTOCs is experimentally challenging due to the requirement of reversing the time evolution of systems. Here we apply Floquet engineering to investigate operator spreading in a superconducting 10-qubit chain. Floquet engineering provides an effective way to tune the coupling strength between nearby qubits, which is used to demonstrate quantum walks with tunable couplings, reversed time evolution, and the measurement of OTOCs. A clear light-cone-like operator propagation is observed in the system with multiple excitations, and has a nearly equal velocity as the single-particle quantum walk. For the butterfly operator that is nonlocal (local) under the Jordan-Wigner transformation, the OTOCs show distinct behaviors with (without) a signature of information scrambling in the near integrable system.

Introduction.—Spreading of quantum operators, probed by out-of-time-order correlators (OTOCs) [1–8], is a new viewpoint to study the dynamics of quantum many-body systems. For instance, it is closely related to the Lieb-Robinson bound [9, 10] in local quantum systems and information scrambling in quantum chaotic systems [1–3, 11–14]. Given two local operators $\hat{W}$ and $\hat{V}$, the OTOC with a pure state $|\psi_0\rangle$ is defined as [5]

$$C(t) = \langle\psi_0|\hat{W}(t)\hat{V}\hat{W}^\dagger(t)\hat{V}^\dagger|\psi_0\rangle, \qquad (1)$$

where $\hat{W}(t) = e^{i\hat{H}t}\hat{W}e^{-i\hat{H}t}$ is the butterfly operator, and $\hat{H}$ is the system Hamiltonian. The OTOC is related to the commutator between $\hat{W}(t)$ and $\hat{V}$. In a dynamical process, it usually starts from unity where two operators fully commute, and decays when they no longer commute and the system may become scrambled [6, 7]. To probe $C(t)$, one generally needs to reverse the time evolution of the system [4, 15–20], which is experimentally very challenging [21]. In the *digital* quantum simulation paradigm [22, 23], the dynamics of quantum many-body systems can be digitalized via a series of quantum gates according to the Trotter-Suzuki decomposition, and the reversed time evolution can be easily implemented in a similar way. These have been investigated in various physical systems such as nuclear magnetic resonance [15, 16], trapped ions [17, 18], and superconducting circuits [19]. On the other hand, it is efficient to encode the reversed dynamics of the target system with a fully-controllable quantum simulator, which is a task of *analog* quantum simulations [22, 23]. In the system with special symmetry, the reversal of time evolution is realized with a combined *digital-analog* scheme in superconducting circuits [20], which nevertheless cannot be simply generalized to other systems without the corresponding symmetry. Hence a method to encode the reversed time evolution of a quantum many-body system in a *full analog*

quantum simulation paradigm is highly desirable.

Floquet engineering, using time-periodic driving, is a powerful tool for the coherent manipulation of quantum manybody states and the control of their dynamics. It has achieved a great success in cold atom systems [24] for a number of studies [25–29]. It has also been applied in superconducting circuits for realizing qubit switch [30], high-fidelity quantum gates [31], quantum state transfer [32], and the model of topological magnon insulators [33]. Floquet driving can be used to tune both the magnitude and phase of the coupling between nearby qubits, thus offering a possible way for reversing the dynamics of a quantum system [24], measuring OTOCs [4], and probing operator spreading.

In this Letter, we present a systematic study of operator spreading using Floquet engineering in a 1D array of 10 superconducting qubits. By precisely adjusting the ac magnetic flux at specific qubits, we are able to tune the coupling strength of nearby qubits and demonstrate the single-photon quantum walk with varying coupling, reversed time evolution, and the measurement of OTOCs. The Pauli operators $\hat{\sigma}^z$ and $\hat{\sigma}^x$ are taken as butterfly operators, which are local and nonlocal under the Jordan-Wigner transformation, respectively. We show that, with multiple excitations, a clear light-cone-like operator propagation can be observed with a velocity nearly equal to the group velocity of single-photon quantum walks. The OTOC with $\hat{W} = \hat{\sigma}^z$ shows a revival to the initial value after a quick decay and finally approaches zero, which characterizes the nonthermalized process in the absence of scrambling. In contrast, no such revival is observed for the OTOC with $\hat{W} = \hat{\sigma}^x$, showing a signature of scrambling. Our results demonstrate distinct behaviors of OTOCs in the nearly integrable system, some of which resemble those in nonintegrable chaotic systems [6, 7].

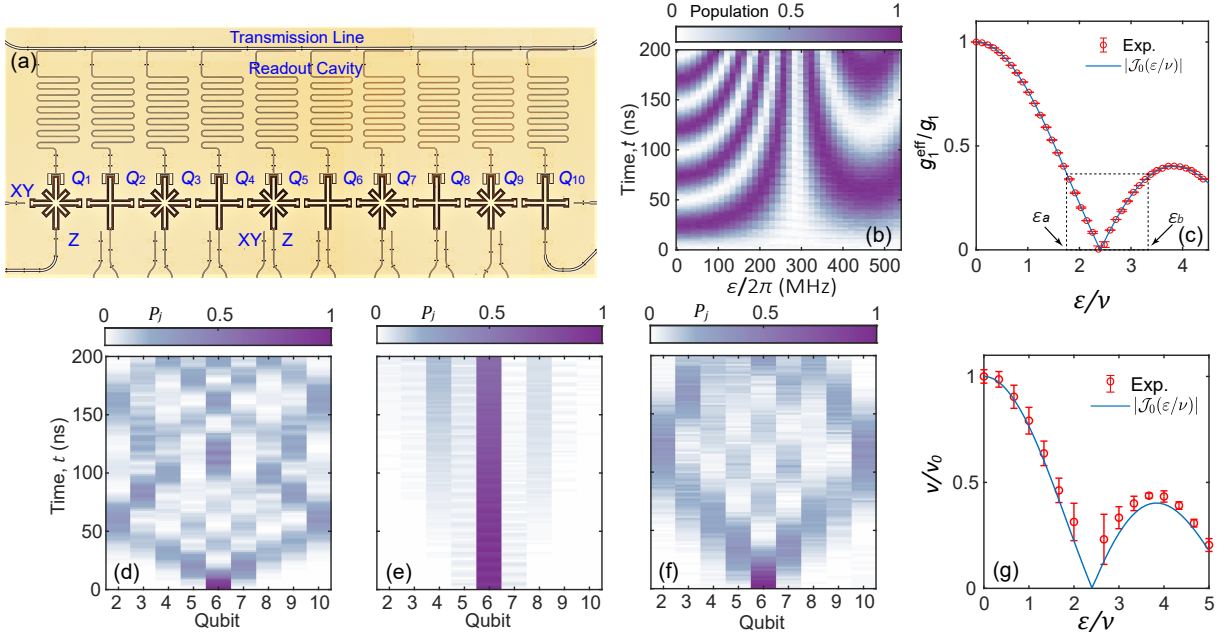*Experimental setup and protocol.*—Superconducting qubits

FIG. 1. Device and quantum walk with tunable coupling. (a) Optical micrograph of the superconducting processor containing 10 transmon qubits arranged into a chain. Each qubit has a microwave line for the XY control, a flux bias line for the Z control, and a readout resonator for measurement. The NN qubits are coupled capacitively with almost the same strength [49]. The parameters of the device are presented in the Supplemental Material (SM) in detail [49]. (b) Experimental results of excitation oscillation between Q_1 and Q_2. The two qubits are prepared in the initial state of $|01\rangle$, and ac magnetic flux is applied on Q_1 with an amplitude ε. The color bar represents the expectation value of the photon number of Q_1. (c) Experimental coupling strength g_1^{eff} versus ac magnetic flux amplitude ε, which satisfies $g_j^{\text{eff}}/g_1 \approx \mathcal{J}_0(\varepsilon/\nu)$. Two arrows indicate the values, ε_a and ε_b, used in the measurement of OTOCs for the forward and backward time evolution, respectively. Single-photon quantum walks for (d) $\varepsilon/2\pi = 120$ MHz, (e) $\varepsilon/2\pi = 288.6$ MHz, and (f) $\varepsilon/2\pi = 400$ MHz, observed on Q_2-Q_{10} with the initial state $|000010000\rangle$. (g) Normalized group velocity v/v_0 of photon propagation versus ε/ν, where $v_0 = 117 \pm 4$ sites/μs corresponds to the value with $\varepsilon = 0$ [49]. The error bar is estimated by fitting errors. Each point is the average result of $8,000$ single-shot readouts.

can be manipulated individually as well as simultaneously, which provide a convenient platform for simulating quantum many-body systems [34–48]. Our experiment is performed on a 1D array of 10 coupled transmon qubits, shown in Fig. 1(a). In the rotating frame with a common frequency, the system is described by the 1D Bose-Hubbard model [38, 41, 43]

$$\hat{H}(t) = \sum_{j=1}^{9} g_j(\hat{a}_j^\dagger \hat{a}_{j+1} + \text{h.c.}) + \sum_{j=1}^{10} \omega_j(t)\hat{n}_j$$
$$+ \sum_{j=1}^{10} \frac{U_j}{2}\hat{n}_j(\hat{n}_j - 1), \tag{2}$$

where $\hat{a}_j^\dagger$ ($\hat{a}_j$) is the bosonic creation (annihilation) operator, $\hat{n}_j = \hat{a}_j^\dagger \hat{a}_j$ is the number operator, U_j is the on-site interaction, and g_j is the nearest-neighbor (NN) coupling strength. In our experiment, we bias the qubit frequency with ac magnetic flux, i.e., we have $\omega_j(t) = \varepsilon_j \cos(\nu t)$, with ν and ε_j being the ac frequency and amplitude, respectively. Thus $\hat{H}(t)$ describes a Floquet system satisfying $\hat{H}(t) = \hat{H}(t+T)$ with a period of $T = 2\pi/\nu$ [49]. When $\nu \gg g_j$, under the hard-core boson approximation with $|U| \gg g_j$, we obtain an effective

time-independent Hamiltonian [24]

$$\hat{H}_{\text{eff}} = \sum_{j=1}^{9} g_j^{\text{eff}}(\hat{\sigma}_j^+ \hat{\sigma}_{j+1}^- + \hat{\sigma}_{j+1}^+ \hat{\sigma}_j^-), \tag{3}$$

where $\hat{\sigma}^\pm = (\hat{\sigma}^x \pm i\hat{\sigma}^y)/2$ with $\hat{\sigma}^{x,y,z}$ being Pauli matrices. The effective coupling strength has the form [24]

$$g_j^{\text{eff}} \approx g_j \mathcal{J}_0\left(\frac{\varepsilon_j - \varepsilon_{j+1}}{\nu}\right), \tag{4}$$

where $\mathcal{J}_0(x)$ is the Bessel function of order zero.

We tune the effective coupling strength between NN qubits by changing ε_j with fixing $\nu/2\pi = 120$ MHz. Figure 1(b) shows the experimental results of the excitation oscillation between Q_1 and Q_2, where the ε-dependent oscillation period can be seen. Using the Fourier transformation, we obtain the effective coupling strength as a function of ε, plotted in Fig. 1(c), which fits well with Eq. (4). In order to have a common coupling strength between each NN qubit pair, we only drive the odd qubits with the same amplitude $|\varepsilon_j| = \varepsilon$, so the coupling strength approximates $g_j \mathcal{J}_0(\varepsilon/\nu)$. In addition, we stagger the phase of the applied flux with $\varepsilon_1, \varepsilon_5, \varepsilon_9 = \varepsilon$ and $\varepsilon_3, \varepsilon_7 = -\varepsilon$ to partly reduce the unwanted next-nearest-neighbor (NNN) coupling [49]. Hence we are able to set identical coupling strength for each NN qubit pair with adjustable values from positive to negative.
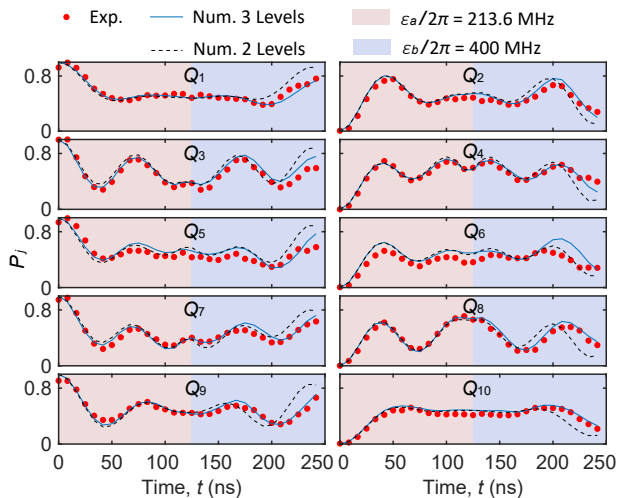
FIG. 2. Reversed time evolution of the 10-qubit chain with the initial state |1010101010⟩, realized by using ε_a and ε_b for the time before and after 125 ns, respectively. Symbols are the experimental results. Solid and dashed lines are the calculated results based on the Hamiltonian in Eq. (2) by considering three and two energy levels for each qubit, respectively.

Quantum walks with tunable coupling.—The quantum walk is a fundamental process for quantum simulation and computation [41, 43, 56–58]. Figures 1(d)-(f) show the experimental observation in a 9-qubit system ($Q_2 - Q_{10}$) with varying effective coupling strength. The experiment starts with all qubits biased at their idle points, and the central qubit Q_6 is excited from the ground state |0⟩ to the first-excited state |1⟩ by an X_π gate to prepare an initial state |000010000⟩ [49]. Afterwards, they are biased to the same frequency and the periodic driving is applied. The system then evolves with almost homogeneous coupling strength between NN qubits. The photon density distribution P_j is measured after the system's evolving for a time t, where $P_j(t) := \langle\psi(t)|\hat\sigma_j^+\hat\sigma_j^-|\psi(t)\rangle$ with $|\psi(t)\rangle$ being the wave function at time t. Figure 1(d) shows the result for $\varepsilon/2\pi = 120$ MHz, which displays a single-photon light-cone-like propagation [41, 43] in both the left and right directions.

We find that the propagation velocity v decreases with increasing ε and vanishes at about $\varepsilon/2\pi \approx 288.6$ MHz ($\varepsilon/\nu \approx 2.4$), corresponding to the first zero of $\mathcal{J}_0$. At this point, the effective NN coupling reduces to zero, leading to dynamic localization [25–27] as illustrated in Fig. 1(e). Further increasing ε results in reappearing of the linear propagation, see Fig. 1(f) for the case of $\varepsilon/2\pi = 400$ MHz. In Fig. 1(g), we show the normalized group velocity v/v_0 versus ε/ν, where $v_0 = 117\pm4$ sites/μs is the value at $\varepsilon = 0$. It can be seen that the data are also well described by the 0-th Bessel function, and the difference mainly originates from the unwanted NNN coupling [49]. Specifically, the group velocity for $\varepsilon/2\pi = 400$ MHz is $v = 46 \pm 4$ sites/μs, which will be compared with the operator spreading velocity below. These results indicate a free single-photon propagation [41, 43] that is limited by the Lieb-Robinson bound [9, 10].

Reversed time evolution.—Reversing the dynamics of a quantum many-body system is of great interest and facilitates the OTOC measurement [5, 20]. Equation (4) indicates that the effective coupling g_j^{eff} can be positive or negative. For single-photon quantum walks, the last term in Eq. (2) vanishes, so the system is governed by the Hamiltonian (3). In this case, the time evolution can be precisely reversed by changing the sign of the Hamiltonian. However, OTOCs provide a technique for studying operator spreading and quantum information propagation in systems with multi-particle filling, which cannot be probed via single-particle propagation. Hence we will focus on the multi-photon system and discuss the effect of high-level occupations.

To observe the reversed time evolution, we choose the initial state as the Néel state |1010101010⟩. The system evolves with a driving amplitude $\varepsilon = \varepsilon_a = 213.6$ MHz for the first 125 ns and with $\varepsilon = \varepsilon_b = 400$ MHz for the last 125 ns. Here we have $\mathcal{J}_0(\varepsilon_a/\nu) = -\mathcal{J}_0(\varepsilon_b/\nu)$, corresponding to $g_j^{\text{eff}} \approx \pm 4$ MHz for ε_a and ε_b, respectively, as indicated by arrows in Fig. 1(c). The experimental results, plotted in Fig. 2 as symbols, are fairly reproduced by numerical simulations (lines). We can see that $P_j(t)$ is nearly symmetric about $t = 125$ ns during the time evolution, demonstrating that two effective time-independent Hamiltonians are almost opposite in sign.

OTOCs and operator spreading.—To measure OTOCs and probe operator spreading, we consider two cases [6, 7]. First, we choose $\hat W = \hat\sigma_{10}^z$, $\hat V = \hat\sigma_j^z$ ($j = 1,...,10$), and the initial state is $|\psi_1\rangle = |0101010101\rangle$. Since $\hat V|\psi_1\rangle = \hat\sigma_j^z|\psi_1\rangle = -(-1)^j|\psi_1\rangle$, from Eq. (1), the corresponding OTOC reads $C_j^{\text{ZZ}}(t) = -(-1)^j\langle\phi_z(t)|\hat\sigma_j^z|\phi_z(t)\rangle$, where $|\phi_z(t)\rangle = \hat\sigma_{10}^z(t)|\psi_1\rangle$ [16]. Second, we let $\hat W = \hat\sigma_{10}^x$, $\hat V = \hat\sigma_j^x$ ($j = 1,...,10$), and the initial state is $|\psi_2\rangle = |{+}{+}{+}{+}{+}{+}{+}{+}{+}{+}\rangle$, where |+⟩ is the eigenstate of $\hat\sigma^x$ with an eigenvalue +1. Similarly, the OTOC is measured as $C_j^{\text{XX}}(t) = \langle\phi_x(t)|\hat\sigma_j^x|\phi_x(t)\rangle$, where $|\phi_x(t)\rangle = \hat\sigma_{10}^x(t)|\psi_2\rangle$ [16]. In the experiment, we first set $\varepsilon = \varepsilon_a$ and let the system evolve for a time t from the initial state. Then we apply a Z (or X) gate on Q_{10} and let the system evolve reversely for time t by setting $\varepsilon = \varepsilon_b$. Finally, we measure the observable $\hat\sigma_j^z$ (or $\hat\sigma_j^x$) to evaluate OTOC.

The experimental and numerical results of C_j^{ZZ} are presented in Fig. 3. We can observe a clear light-cone-like operator propagation in Fig. 3(a). The velocity of operator spreading is calculated to be 40 ± 7 sites/μs [49], which almost equals to the group velocity of single-photon quantum walks with the identical coupling strength. The small difference between these two velocities mainly comes from the NNN coupling, which enlarges the group velocity of single-photon quantum walks [49]. These results demonstrate that operator spreading with the local Hamiltonian is also limited by the Lieb-Robinson bound. The measured OTOCs are also plotted in Fig. 3(c) as symbols. They show a clear decay at the early stage and then revive almost back to the initial value of +1 for qubits near Q_{10}, which implies the absence of information scrambling. This can be explained considering that the effective Hamiltonian in Eq. (3) is integrable [3, 15]. It maps
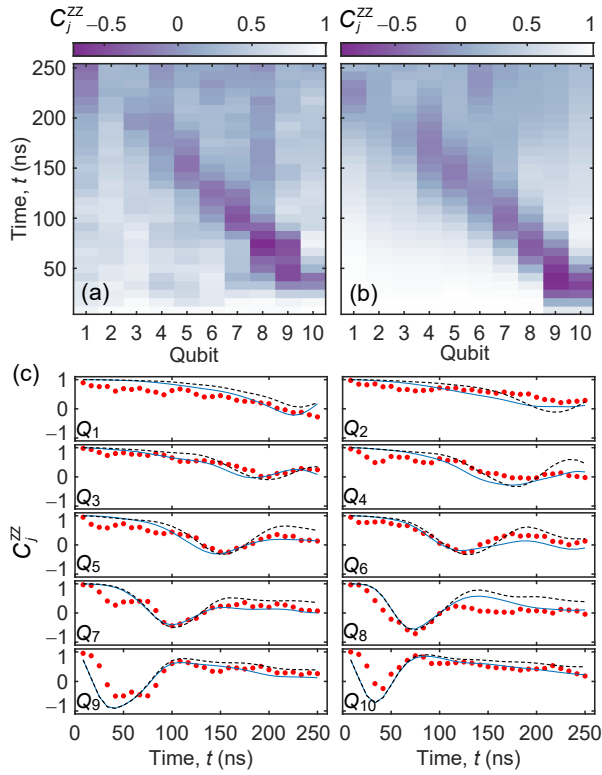
FIG. 3. (a) Experimental results of C_j^{ZZ}, with the initial state $|0101010101\rangle$ and operators $\hat{W} = \hat{\sigma}_{10}^z$, $\hat{V} = \hat{\sigma}_j^z$ ($j = 1, ..., 10$). The post-selection is applied due to the $U(1)$ symmetry, i.e., only the single-shot results that have the same number of bosons as the initial state are considered. (b) Numerical results considering ZZ interaction between NN qubits. (c) Comparison between experimental C_j^{ZZ} (symbols) and two calculated results using $\hat{H}_{\text{eff}}$ (dashed lines) and considering ZZ interaction (solid lines).
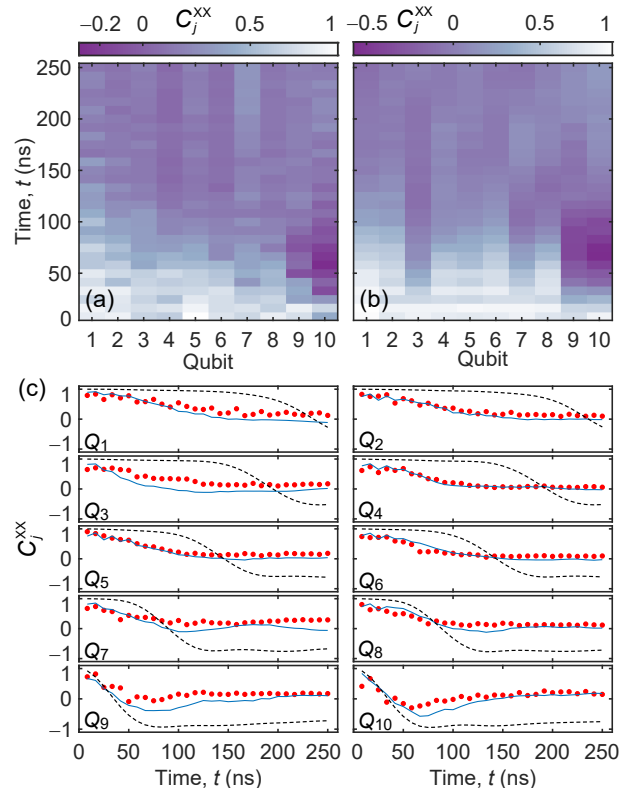
FIG. 4. (a) Experimental results of C_j^{XX} with the initial state $|++++++++++\rangle$ and operators $\hat{W} = \hat{\sigma}_{10}^x$, $\hat{V} = \hat{\sigma}_j^x$ ($j = 1, ..., 10$). (b) Numerical results considering the qubit third energy level. (c) Comparison between experimental C_j^{XX} (symbols) and two numerical results using two (dashed lines) and three (solid lines) qubit levels.

to free fermions under the Jordan-Wigner transformation and the $\hat{\sigma}^z$ operator does not change under the map. Finally, C_j^{ZZ} gradually decays to zero at later time, indicating that $|\phi_z(t)\rangle$ tends to a steady state. Since the initial state is in the half-filling sector and $|\phi_z(t)\rangle$ is spin conserved, C_j^{ZZ} represented by spin distribution will finally stabilize at zero.

These results show that OTOCs can well characterize the nonthermalized process and operator spreading in the multi-particle system. The effect of the last term in Eq. (2) can also be seen, where it is not time reversible under the Floquet driving leading to a discrepancy from ideal time reversal [20]. For the results in Fig. 2, numerical simulations show that the population of the second-excited state varies with a maximum value up to 10%, as compared to those of the first-excited state around 50%. In Fig. 2, we present two results calculated by three- and two-level approximation of $\hat{H}(t)$, respectively. The result considering three levels is closer to experimental data. For the OTOC results in Fig. 3, where the post-selection is used, we take into account the influence of the third level through ZZ interaction [20, 59]. In Fig. 3(c), we can find that this numerical result is closer to experimental data than those calculated using $\hat{H}_{\text{eff}}$ in Eq. (3) [49].

The corresponding results of C_j^{XX} are shown in Fig. 4. A significant difference from C_j^{ZZ} is that no similar revival back to +1 is observed, which suggests the presence of scrambling with the $\hat{\sigma}^x$ butterfly operator [6, 7]. In the results, several features are blurred due to the high level participation [20]. The solid lines in Fig. 4(c) are the results calculated by considering the qubit third level [49], showing a satisfactory fit to experimental data. In addition, the results calculated by using two levels (dashed lines) demonstrate clear properties that C_j^{XX} would have: First, the wavefront of OTOC can be better defined and propagates to the other edge of the qubit chain at a time nearly equal to that for C_j^{ZZ}. Second, C_j^{XX} decreases at early times from +1 to -1 and almost retains in the rest of time range up to 250 ns. Here, the difference between butterfly operators $\hat{\sigma}^z$ and $\hat{\sigma}^x$ is that the former is local under the Jordan-Wigner transformation, whereas the latter maps to nonlocal Pauli-string operators giving rise to the behavior characteristic of scrambling [6, 7]. We emphasize that the scrambling here is fundamentally different from that in nonintegrable systems, in which it persists in a long timescale [3]. For both integrable and nonintegrable systems, the length of the string operators would increase linearly until approaching the system size. Afterwards, it will start to decrease and saturate for

the two systems, respectively [2]. In SM [49], we show the periodic behavior of C_j^{XX} by numerical simulation in a larger timescale, which demonstrates the existence of string operator shrinking in our near integrable system.

Summary and outlook.—We have used Floquet engineering, a full analog method, for probing operator spreading. Quantum walks with tunable coupling, reversed time evolution, and the measurement of OTOCs were demonstrated in a superconducting qubit chain. We observed a linear propagation of quantum operator with a velocity nearly equal to the group velocity of single-photon quantum walk, and also found that the OTOCs behave differently between $\hat{\sigma}^z$ and $\hat{\sigma}^x$ butterfly operators. The method may have further applications for the simulation of quantum many-body physics, e.g., quantum information scrambling and thermalization in nonintegrable systems [1–3, 11–14], dynamics of systems with weak integrability breaking [60, 61], artificial gauge field [28], topological band theory [62], and topological edge mode [49] in the Su-Schrieffer-Heeger model [63].

* These authors contributed equally to this work.
† hfyu@baqis.ac.cn
‡ dzheng@iphy.ac.cn
§ hfan@iphy.ac.cn
¶ spzhao@iphy.ac.cn

[1] S. H. Shenker, and D. Stanford, Black holes and the butterfly effect, J. High Energy Phys. 03 (2014) 067.

[2] D. A. Roberts, D. Stanford, and L. Susskind, Localized shocks, J. High Energy Phys. 03 (2015) 051.

[3] P. Hosur, X. L. Qi, D. A. Roberts, and B. Yoshida, Chaos in quantum channels J. High Energy Phys. 02 (2016) 004.

[4] H. Shen, P. Zhang, R. Fan, and H. Zhai, Out-of-time-order correlation at a quantum phase transition, Phys. Rev. B 96, 054503 (2017).

[5] B. Swingle, Unscrambling the physics of out-of-time-order correlators Nat. Phys. 14, 988 (2018).

[6] C.-J Lin and O. I. Motrunich, Out-of-time-ordered correlators in a quantum Ising chain, Phys. Rev. B 97, 144304 (2018).

[7] C.-J Lin and O. I. Motrunich, Out-of-time-ordered correlators in short-range and long-range hard-core boson models and in the Luttinger-liquid model, Phys. Rev. B 98, 134305 (2018).

[8] M.K. Joshi, A. Elben, B. Vermersch, T. Brydges, C. Maier, P. Zoller, R. Blatt, and C. F. Roos, Quantum information scrambling in a trapped-ion quantum simulator with tunable range interactions, Phys. Rev. Lett 124, 240505 (2020).

[9] E. H. Lieb and D. W. Robinson, The finite group velocity of quantum spin systems, Commun. Math. Phys. 28, 251 (1972).

[10] S. Bravyi, M. B. Hastings, F. Verstraete, Lieb-Robinson bounds and the generation of correlations and topological quantum order, Phys. Rev. Lett. 97, 050401 (2006).

[11] A. Kitaev, *A simple model of quantum holography, in Proceedings at KITP, 2015* (2015).

[12] A. Bohrdt, C. B. Mendl, M. Endres, and M. Knap, Scrambling and thermalization in a diffusive quantum many-body system, New J. Phys. 19, 063001 (2017).

[13] A. Nahum, S. Vijay, and J. Haah, Operator spreading in random unitary circuits, Phys. Rev. X 8, 021014 (2018).

[14] C. W. von Keyserlingk, T. Rakovszky, F. Pollmann, and S. L. Sondhi, Operator hydrodynamics, OTOCs, and entanglement growth in systems without conservation laws, Phys. Rev. X 8, 021013 (2018).

[15] J. Li, R. Fan, H. Wang, B. Ye, B. Zeng, H. Zhai, X. Peng, and J. Du, Measuring out-of-time-order correlators on a nuclear magnetic resonance quantum simulator, Phys. Rev. X 7, 031011 (2017).

[16] X. Nie, B.-B. Wei, X. Chen, Z. Zhang, X. Zhao, C. Qiu, Y. Tian, Y. Ji, T. Xin, D. Lu , and J. Li, Experimental observation of equilibrium and dynamical quantum phase transitions via out-of-time-ordered correlators, Phys. Rev. Lett. 124, 250601 (2020).

[17] M. Gärttner, Justin G. Bohnet, A. Safavi-Naini, M. L. Wall, J. J. Bollinger, and A. M. Rey, Measuring out-of-time-order correlations and multiple quantum spectra in a trapped-ion quantum magnet, Nat. Phys. 13, 781 (2017).

[18] K. A. Landsman, C. Figgatt, T. Schuster, N.M. Linke, B. Yoshida, N. Y. Yao, and C. Monroe, Verified quantum information scrambling, Nature (London) 567, 61 (2019).

[19] X. Mi *et al.*, Information scrambling in computationally complex quantum circuits, Science 374, 1479 (2021).

[20] J. Braumüller, A.H. Karamlou, Y. Yanay, B. Kannan, D. Kim, M. Kjaergaard, A. Melville, B. M. Niedzielski, Y. Sung, A. Vepsäläinen, R. Winik, J. L. Yoder, T. P. Orlando, S. Gustavsson, C. Tahan, and W. D. Oliver, Probing quantum information propagation with out-of-time-ordered correlators, Nat. Phys. 18, 172 (2022).

[21] Protocols without reversing the time evolution of the system can be found in Refs. [4, 8].

[22] I. Buluta and F. Nori, Quantum simulators, Science 326, 108 (2009).

[23] I. M. Georgescu, S. Ashhab, and F. Nori, Quantum simulation, Rev. Mod. Phys. 86, 153 (2014).

[24] A. Eckardt, Colloquium: Atomic quantum gases in periodically driven optical lattices, Rev. Mod. Phys. 89, 011004 (2017).

[25] D. H. Dunlap, and V. M. Kenkre, Dynamic localization of a charged particle moving under the influence of an electric field, Phys. Rev. B 34, 3625 (1986).

[26] H. Lignier, C. Sias, D. Ciampini, Y. Singh, A. Zenesini, O. Morsch, and E. Arimondo, Dynamical control of matter-wave tunneling in periodic potentials, Phys. Rev. Lett 99, 220403 (2007).

[27] A. Eckardt, M. Holthaus, H.Lignier, A. Zenesini, D. Ciampini, O. Morsch, and E. Arimondo, Exploring dynamic localization with a Bose-Einstein condensate, Phys. Rev. Lett 79, 013611 (2009).

[28] J. Dalibard, F. Gerbier, G. Juzeliūnas, and P. Öhberg, Collo-

quium: Artificial gauge potentials for neutral atoms, Rev. Mod. Phys. **85**, 1523 (2011).

[29] G. Jotzu, M. Messer, R. Desbuquois, M. Lebrat, T. Uehlinger, D. Greif, and T. Esslinger, Experimental realization of the topological Haldane model with ultracold fermions, Nature **515**, 237 (2014).

[30] Y. Wu, L. Yang, M. Gong, Y. Zheng, H. Deng, Z. Yan, Y. Zhao, K. Huang, A. D. Castellano, W. J. Munro, K. Nemoto, D. Zheng, C. P. Sun, Y. X. Liu, X. Zhu, and L. Lu, An efficient and compact switch for quantum circuits, npj Quantum Inf. **4**, 50 (2018).

[31] M. Reagor, C. B. Osborn, N. Tezak, A. Staley, G. Prawiroatmodjo, M. Scheer *et al.*, Demonstration of universal parametric entangling gates on a multi-qubit lattice, Sci. Adv. **4**, eaao3603 (2018).

[32] X. Li, Y. Ma, J. Han, T. Chen, Y. Xu, W. Cai, H.Wang, Y. P. Song, Z.-Y. Xue, Z.-Q. Yin, and L. Sun, Perfect quantum state transfer in a superconducting qubit chain with parametrically tunable couplings, Phys. Rev. Applied **10**, 054009 (2018).

[33] W. Cai, J. Han, F. Mei, Y. Xu, Y. Ma, X. Li, H. Wang, Y. P. Song, Z.-Y. Xue, Z. Yin, S. Jia, and L. Sun, Observation of topological magnon insulator states in a superconducting circuit, Phys. Rev. Lett. **124**, 080501 (2019).

[34] Y. Salathé, M. Mondal, M. Oppliger, J. Heinsoo, P. Kurpiers, A. Potočnik, A. Mezzacapo, U. Las Heras, L. Lamata, E. Solano, S. Filipp, and A. Wallraff, Digital quantum simulation of spin models with circuit quantum electrodynamics, Phys. Rev. X **5**, 021027 (2015).

[35] R. Barends, L. Lamata, J. Kelly, L. García-Álvarez, A. G. Fowler, A Megrant, E Jeffrey, T. C. White, D. Sank, J. Y. Mutus, B. Campbell, Yu Chen, Z. Chen, B. Chiaro, A. Dunsworth, I.-C. Hoi, C. Neill, P. J. J. O'Malley, C. Quintana, P. Roushan, A. Vainsencher, J. Wenner, E. Solano, and John M. Martinis, Digital quantum simulation of fermionic models with a superconducting circuit, Nat. Commun. **6**, 7654 (2015).

[36] Y. P. Zhong, D. Xu, P. Wang, C. Song, Q. J. Guo, W. X. Liu, K. Xu, B. X. Xia, C.-Y. Lu, S. Han, J.-W. Pan, and H. Wang, Emulating anyonic fractional statistical behavior in a superconducting quantum circuit, Phys. Rev. Lett. **117**, 110501 (2016).

[37] E. Flurin, V. V. Ramasesh, S. Hacohen-Gourgy, L. S. Martin, N. Y. Yao, and I. Siddiqi, Observing topological invariants using quantum walks in superconducting circuits, Phys. Rev. X **7**, 031023 (2017).

[38] P. Roushan, C. Neill, J. Tangpanitanon, V. M. Bastidas, A. Megrant, R. Barends, Y. Chen, Z. Chen, B. Chiaro, A. Dunsworth, A. Fowler, B. Foxen, M. Giustina, E. Jeffrey, J. Kelly, E. Lucero, J. Mutus, M. Neeley, C. Quintana, D. Sank, A. Vainsencher, J. Wenner, T. White, H. Neven, D. G. Angelakis, and J. Martinis, Spectroscopic signatures of localization with interacting photons in superconducting qubits, Science **358**, 1175 (2017).

[39] K. Xu, J. J. Chen, Y. Zeng, Y. R. Zhang, C. Song, W. X. Liu, Q. J. Guo, P. F. Zhang, D. Xu, H. Deng, K. Q. Huang, H. Wang, X. B. Zhu, D. N. Zheng, and H. Fan, Emulating many-body localization with a superconducting quantum processor, Phys. Rev. Lett. **120**, 050507 (2018).

[40] C. Song, D. Xu, P. Zhang, J. Wang, Q. Guo, W. Liu, K. Xu, H. Deng, K. Huang, D. Zheng, S.-B. Zheng, H. Wang, X. Zhu, C.-Y. Lu, and J.-W. Pan, Demonstration of topological robustness of anyonic braiding statistics with a superconducting quantum circuit, Phys. Rev. Lett. **121**, 030502 (2018).

[41] Z. Yan, Y. R. Zhang, M. Gong, Y. Wu, Y. Zheng, S. Li, C. Wang, F. Liang, J. Lin, Y. Xu, C. Guo, L. Sun, C. Z. Peng, K. Xia, H. Deng, H. Rong, J. Q. You, F. Nori, H. Fan, X. Zhu, and

J.-W. Pan, Strongly correlated quantum walks with a 12-qubit superconducting processor, Science **364**, 753 (2019).

[42] R. Ma, B. Saxberg, C. Owens, N. Leung, Y. Lu, J. Simon, and D. I. Schuster, A dissipatively stabilized Mott insulator of photons, Nature **566**, 51 (2019).

[43] Y. Ye, Z.-Y. Ge, Y. Wu, S. Wang, M. Gong, Y.-R. Zhang, Q. Zhu, R. Yang, S. Li, F. Liang, J. Lin, Y. Xu, C. Guo, L. Sun, C. Cheng, N. Ma, Z. Y. Meng, H. Deng, H. Rong, C.-Y. Lu, C.-Z. Peng, H. Fan, X. Zhu, and J.-W. Pan, Propagation and localization of collective excitations on a 24-qubit superconducting processor, Phys. Rev. Lett. **123**, 050502 (2019).

[44] X.-Y Guo, C. Yang, Y. Zeng, Y. Peng, H.-K Li, H. Deng, Y.-R Jin, S. Chen, D.-N Zheng, and H. Fan, Observation of a dynamical quantum phase transition by a superconducting qubit simulation, Phys. Rev. Applied **11**, 044080 (2019).

[45] F. Arute, K. Arya, R. Babbush, D. Bacon, J. C. Bardin, R. Barends, R. Biswas, S. Boixo, F. G.Brandao, D. A. Buell *et al.*, Quantum supremacy using a programmable superconducting processor, Nature (London) **574**, 505 (2019).

[46] K. Xu, Z.-H Sun, W. Liu, Y.-R Zhang, H. Li, H. Dong, W. Ren, P. Zhang, F. Nori, D. Zheng, H. Fan, H. Wang, Probing dynamical phase transitions with a superconducting quantum simulator, Sci. Adv. **6**, eaba4935 (2020).

[47] X.-Y Guo, Z.-Y. Ge, H. Li, Z. Wang, Y.-R. Zhang, P. Song, Z. Xiang, X. Song, Y. Jin, L. Lu, K. Xu, D. Zheng, and H. Fan, Observation of Bloch oscillations and Wannier-Stark localization on a superconducting quantum processor, npj Quantum Inf. **7**, 51 (2021).

[48] Q. Guo, C. Cheng, Z.-H. Sun, Z. Song, H. Li, Z. Wang, W. Ren, H. Dong, D. Zheng, Y.-R. Zhang, R. Mondaini, H. Fan, and H. Wang, Observation of energy-resolved many-body localization, Nat. Phys. **17**, 234 (2021).

[49] See Supplemental Material...for...,which includes Refs. [50–55].

[50] J. Koch, T. M. Yu, J. Gambetta, A. A. Houck, D. I. Schuster, J. Majer, A. Blais, M. H. Devoret, S. M. Girvin, and R. J. Schoelkopf, Charge-insensitive qubit design derived from the cooper pair box, Phys. Rev. A **76**, 042319 (2007).

[51] R. Barends, J. Kelly, A. Megrant, D. Sank, E. Jeffrey, Y. Chen, Y. Yin, B. Chiaro, J. Mutus, C. Neill, P. O'Malley, P. Roushan, J. Wenner, T. C. White, A. N. Cleland, and J. M. Martinis, Coherent Josephson qubit suitable for scalable quantum integrated circuits, Phys. Rev. Lett. **111**, 080502 (2013).

[52] Z. Chen, A. Megrant, J. Kelly, R. Barends, J. Bochmann, Y. Chen, B. Chiaro, A. Dunsworth, E. Jeffrey, J. Y. Mutus, P. J. J. O'Malley, C. Neill, P. Roushan, D. Sank, A. Vainsencher, J. Wenner, T. C. White, A. N. Cleland, and J. M. Martinis, Fabrication and characterization of aluminum airbridges for superconducting microwave circuits, Appl. Phys. Lett. **104**, 052602 (2014).

[53] M. D. Reed, *Entanglement and Quantum Error Correction with Superconducting Qubits*, Ph.D. thesis (2013).

[54] J. Ku, X. Xu, M. Brink, D. C. McKay, J. B. Hertzberg, M. H. Ansari, and B. L. T. Plourde. Suppression of Unwanted ZZ Interactions in a Hybrid Two-Qubit System, Phys. Rev. Lett. **125**, 200504 (2020).

[55] C. Song, K.Xu, W. Liu, C.-p. Yang, S. B. Zheng, H. Deng, Q. Xie, K. Huang, Q. Guo, L. Zhang, P. Zhang, D. Xu, D. Zheng, X. Zhu, H. Wang, Y.-A. Chen, C.-Y. Lu, S. Han, and J.-W. Pan, 10-Qubit Entanglement and Parallel Logic Operations with a Superconducting Circuit, Phys. Rev. Lett. **119**, 180511 (2017).

[56] M. Gong, S. Wang, C. Zha, M.-C. Chen, H.-L. Huang, Y. Wu, Q. Zhu, Y. Zhao, S. Li, S. Guo, H. Qian, Y. Ye, F. Chen, C. Ying, J. Yu, D. Fan, D. Wu, H. Su, H. Deng, H. Rong, K. Zhang, S.

Cao, J. Lin, Y. Xu, L. Sun, C. Guo, N. Li, F. Liang, V. M. Bastidas, K. Nemoto, W. J. Munro, Y.-H. Huo, C.-Y. Lu, C.-Z. Peng, X. Zhu, and J.-W. Pan, Quantum walks on a programmable two-dimensional 62-qubit superconducting processor, Science **373**, 948 (2021).

[57] M. S. Underwood, and D. L. Feder, Bose-Hubbard model for universal quantum-walk-based computation, Phys. Rev. A **85**, 052314 (2012).

[58] A. M. Childs, D. Gosset, and Z. Webb, Universal computation by multiparticle quantum walk, Science **339**, 791 (2013).

[59] D. C. McKay, C. J. Wood, S. Sheldon, J. M. Chow, and J. M. Gambetta, Efficient Z gates for quantum computing, Phys. Rev.

A **96**, 022330 (2017).

[60] A. Polkovnikov, K. Sengupta, A. Silva, and M. Vengalattore, Colloquium: Nonequilibrium dynamics of closed interacting quantum systems, Rev. Mod. Phys. **83**, 863 (2011).

[61] M. Marcuzzi, J. Marino, A. Gambassi, and A. Silva, Prethermalization in a nonintegrable quantum spin chain after a quench, Phys. Rev. Lett. **111**, 197203 (2013).

[62] A. Bansil, H. Lin, and T. Das, Colloquium: Topological band theory, Rev. Mod. Phys. **88**, 021004 (2016).

[63] W. P. Su, J. R. Schrieffer, and A. J. Heeger, Solitons in Polyacetylene, Phys. Rev. Lett. **42**, 1698 (1979).